sciendo

Civil and Environmental Engineering
Vol. 19, Issue 1, 339-347, DOI: 10.2478/cee-2023-0030

# STABILITY OF THE ČACHTICE UNDERGROUND CORRIDORS

Roman BULKO[1,*], Juraj MUŽÍK[1], Monika GWÓŹDŹ - LASOŃ[2], Janusz JURASZEK[2], Andrea SEGALINI[3]

[1] Department of Geotechnics, Faculty of Civil Engineering, University of Žilina, Univerzitná 8215/1, 010 26 Žilina, Slovakia.
[2] Department Civil Engineering, Faculty of Materials, Civil and Environmental Engineering, University of Bielsko-Biala, Willowa 2 43-309 Bielsko-Biała Poland.
[3] Dipartimento di Ingegneria e Architettura, University of Parma, Parco Area delle Scienze 181/a, 43124 Parma, Italy.
[*] corresponding author: roman.bulko@uniza.sk

**Abstract**

At the beginning of the 16th century, the original inhabitants of Čachtice built a large complex of tunnels and cellars under the village, today called the Čachtice underground. The underground protected people from war conflicts, most recently during World War II, as anti-aircraft shelters. Over time, the underground lost its significance. The corridors were walled up, covered with rubble, and collapsed due to construction work. Later, a part of the underground was repaired, and historical events occurred in such a preserved part. Due to a lawsuit, the Čachtice underground was eventually closed to the public, and it was necessary to test the stability of the walls of the Čachtice underground. A 3D model of the underground was created, and three areas were identified in which numerical calculations were performed in Plaxis 2D software. The whole underground is located in loess soil. The Čachtice underground is stable if the conditions do not change diametrically. The calculated factors of safety support this assumption.

**Keywords:**

Stability factor;
Čachtice underground;
Loess clay;
Plaxis;
Mohr's circles.

## 1 Introduction

The Čachtice underground spreads like a cobweb under the whole of Čachtice. The corridors began to be built during the Orság era, sometime in the early 16th century. The inhabitants built several kilometre-long corridors from the original wine cellars with several floors to protect against Turkish raids. Narrow entrances were necessary for easy defence against enemies when only one armed man could stop an entire regiment of troops. The underground was also adapted for the extended stay of the people, and they had fruit, wine, icehouses with food, and pits with grain stored in it. The underground protected people from war events, most recently during World War II, as anti-aircraft shelters. Gradually, it lost its significance, and the corridors were bricked up, rubbed with rubble, and collapsed due to construction work on the surface. Most of the corridors are irretrievably lost today. Miraculously, the underground beneath the former 16th-century wine mill, which belonged to the Nádašdy family, has been preserved. The manor had protection behind the palace walls, but the servants used the underground under the press. To this day, the Nádašdy coat of arms in the shape of a duck, decorative portals, and various signatures of visitors was preserved in the underground even several centuries ago. The corridors are managed by the Civic Association Čachtice Underground, which adjusts sections of the corridors for inspections. The significant impact of geotourism on historical monuments affected the quality of living in the locality [1]. However, some citizens of the village of Čachtice were not history enthusiasts, and the civic association sued. A static assessment of the walls of the Čachtice underground was prepared.

## 2 Geological composition of the Čachtice underground

The village of Čachtice is located in the southern part of the White Carpathians. The Quaternary consists of eolithic and eolithic-diluvial sediments such as loess and loess clay, Fig. 1. Late-glacial loess clays form a transitional type of cover between loess and polygenetic slope clays. They have a relatively large area in the territory of the Western Carpathians and the adjacent part of the Pannonian Basin. They have developed and been preserved mainly in the foothills of the lowlands, in the hills, where they continuously line the loess occurrences and cover parts of the Lower and Middle Pleistocene alluvial cones and terraces. The thickness of the loess is very variable. It reaches its most significant values at the foot of the slopes, wherein, in some places, the clays form walkable diluvial mantles with a thickness of up to 7 - 10 m. The thicknesses in the lower parts of the slopes, valleys, and edges of the cone bodies are also more pronounced. They most often range in value from 2 to 5 m. The loess clays have a similar morphology and habitus, but their genesis has a different character. Lithological characteristics and storage conditions suggest that eolithic transfer and accumulation were similar to loess, but the post-sedimentation environment was wetter. There was no pollination, but flooding, where pedogenetic changes prevailed with increased clay content and descaling, while iron oxide $FeO_3$ replaced calcium carbonate $CaCO_3$. The predominant component is the clay fraction and the dust to coarse dust fraction. The sites have a loess character or generally contain dusty positions, but loess complexes' typical columnar separation and permeability characteristics are absent. They have low porosity. Due to the cyclical repetition of erosion and sedimentation processes, and the associated regular renewal of slope exposure, loess clays are marked mainly by the lithological composition of the underlying sediments. The colour of the deposits is yellow-grey, yellow-brown, and brown to rusty-grey-leafy. The structure is lumpy till prismatic. Iron and manganese concretions are abundant in them, occasionally also smaller concretions, as well as grey coatings and plugs caused by polymerization processes - leaching of clays into deeper soil layers [2].

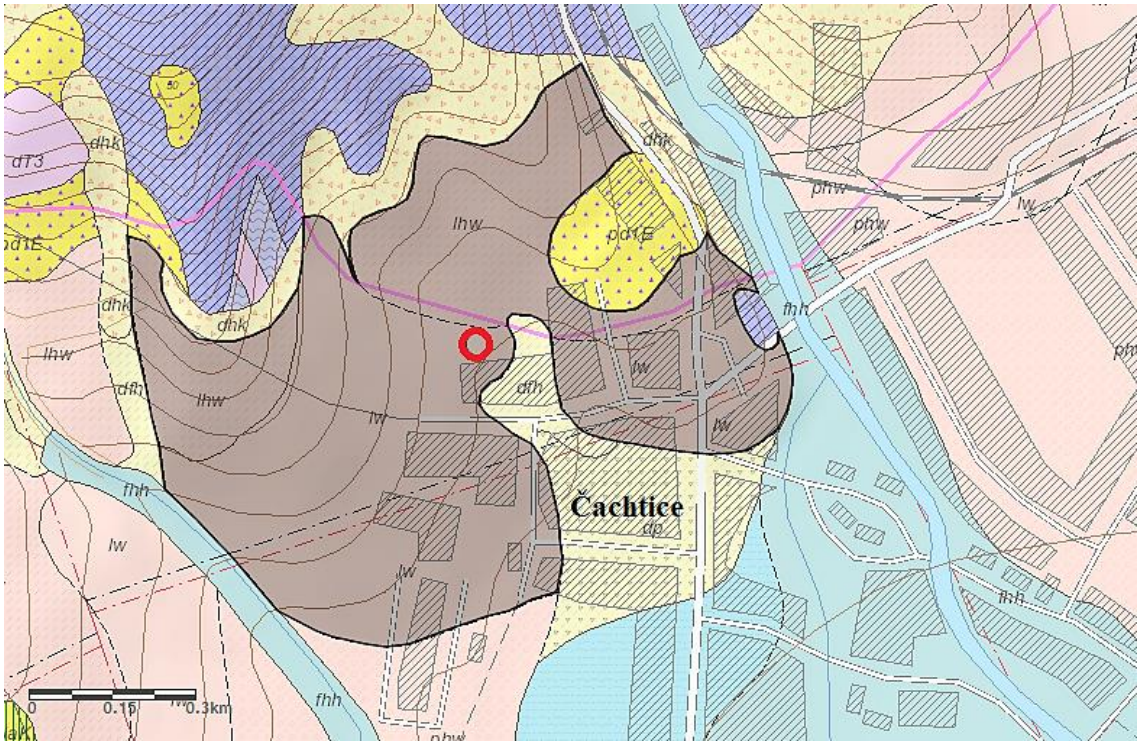


Fig. 1: Geology in the area in question [3].

## 3 Laboratory results of soil tests

Fig. 2 shows the underground corridors plan of the Čachtice. Marks in the figure represent three localities, cross-sections R1 - R3, where the profile was used for stability calculations and one location where soil samples were taken for laboratory evaluation R4. Five intact soil samples and one disturbed soil sample were tested in the geotechnical laboratory of the University of Žilina. Subsequently, laboratory tests were made from these samples determining the mechanical, physical, and descriptive properties of soils following:

- STN 72 1001: Classification of soil and rock.
- STN 72 1010: Determination of earth volume mass. Laboratory and field methods.
- STN 72 1011: Laboratory determination of apparent density of solid particles of soils.
- STN 72 1012: Laboratory determination of moisture content of soils.
- STN 72 1013: Laboratory determination of plasticity limit of soils.
- STN 72 1014: Laboratory determination of liquid limit. Casagrande method.
- STN 72 1027: Laboratory determination of soil compressibility in the oedometer apparatus.
- STN 72 1030: Laboratory direct shear box drained test of soils.

The resulting loess properties are shown in Table 1. In concrete structures, loess can resemble foam concrete in its design. Both materials have high porosity. For example, the deformation properties of foam concrete were investigated by Vlček et al. [4]. From the results of laboratory tests and by STN 73 1001, we classify the soil as clay with low plasticity. In terms of genesis, these are coiled fine-grained so-called loess. According to the indices, $I_{mp}$ = 8.31 % and $M_{pr}$ = 83.12 mm·m$^{-1}$, these loesses are highly collapsible [3]. If the coefficient Imp is above 1%, the soil is collapsible. $I_{mp}$ is the collapsibility coefficient, and $M_{pr}$ is the collapsibility modulus calculated as follows:

$$I_{mp} = \frac{\Delta h_p}{h_0}.100\ \%\ , \tag{1}$$

$$M_{pr} = \frac{\Delta h_p}{h_0}\ , \tag{2}$$

where, $\Delta h_p$ is the additional settlement of the sample after flooding with water in mm and $h_0$ is the height of the sample before flooding with water in mm for $I_{mp}$ and in m for $M_{pr}$ [5].

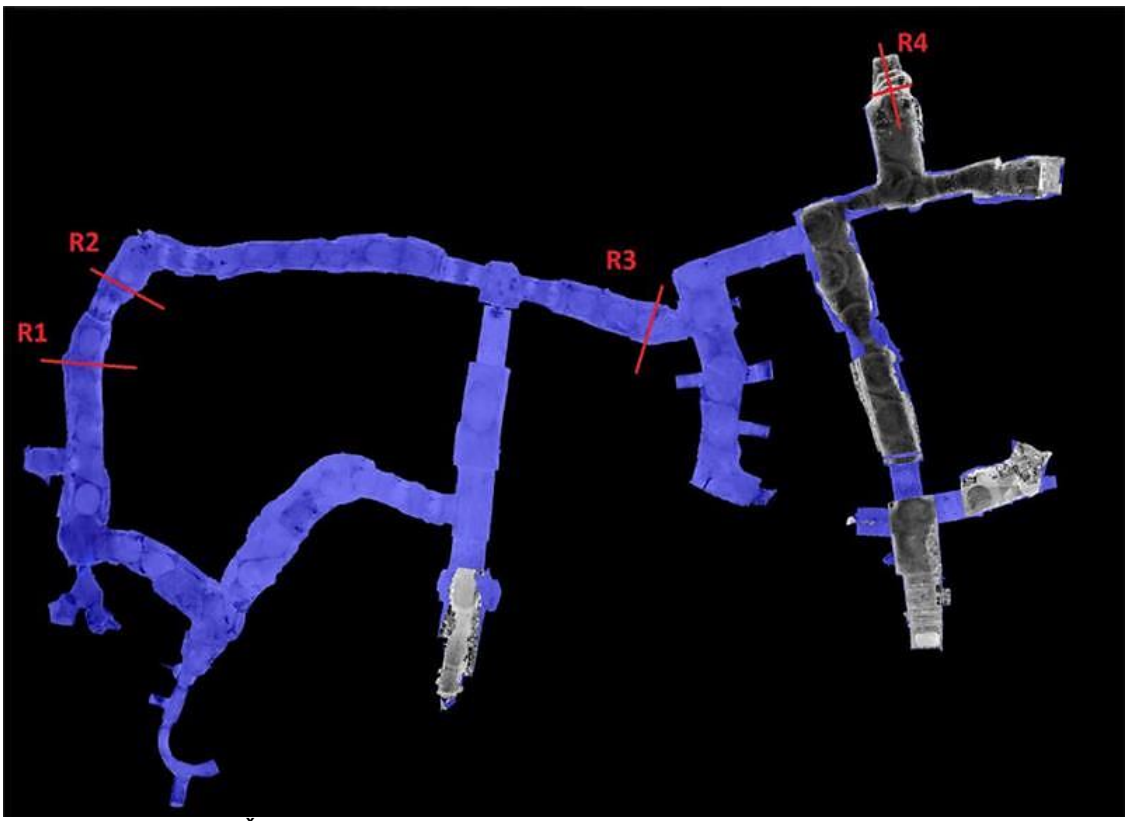


Fig. 2: 3D scan of the Čachtice underground corridors and selected three sites, R1, R2, and R3, for stability calculation; R4 is the soil sampling site.

Nowadays, we can explore hidden objects, cavities, and corridors differently. For example, using georadar, gravimetry, or, if the corridors are already accessible, using a 3D scan, as shown in Fig. 2. By using 3D scanning, we can measure the exact geometry of the object [6, 7].

Table 1: Geotechnical properties of soil from the Čachtice underground investigated in the geotechnical laboratory of the University of Žilina.

| Name | Mark [unit] | Value |
|---|---|---|
| Soil | F6/CL – Loess | |
| Humidity | $w$ [%] | 11.70 |
| Bulk density of soil | $\rho$ [kg/m$^3$] | 1400 |
| The specific density of solid particles | $\rho_s$ [kg/m$^3$] | 2460 |
| Oedometric module | $E_{OED}$ [MPa] | 2.46 |
| Poisson's number | $v$ [-] | 0.4 |
| Porosity number | $e$ [-] | 0.85 |
| Internal friction angle | $\phi_{ef}$ [°] | 23.6 |
| Cohesion | $c_{ef}$ [kPa] | 29 |

## 4 FEM model of the Čachtice underground

The stability of the Čachtice underground was analyzed in 3 selected sections using the finite element code PLAXIS 2D version 8.5. This analysis used two constitutive material models, Linear Elastic and Mohr-Coulomb. The stability calculation was realized in three stages:

- First stage: The areas with the highest stress deviator concentration were identified during the linear model application to localize the potential failure zones and reconstruct the primary stress state.
- Second step: The Mohr-Coulomb constitutive model was adopted to identify the onset of plastic zones.
- Third step: The factor of safety (FS) was calculated as the parameter that describes the stability of a particular cross-section.

According to Eurocode 7: Geotechnical design - Part 1: General rules, verification of the stability for numerical problems, we follow DA3 (design approach 3). The geometry of these sections was obtained from the 3D scanning point cloud and subsequently imported into the PLAXIS 2D program environment. The input data are in Table 2. The input material characteristics of soils are reduced by safety factors of 1.25. The oedometric modulus can vary significantly across the sample types and individual step stresses [8, 9].

Table 2: Soil input parameters F6/CL – Loess.

| Name | Mark [unit] | Linear elastic | Mohr-Coulomb |
|---|---|---|---|
| Unit weight of soil | $\gamma$ [kN/m$^3$] | 14.0 | 14.0 |
| Young module | $E$ [MPa] | 2.0 | - |
| Deformation module | $E_{def}$ [MPa] | - | 2.0 |
| Poisson number | $v$ [-] | 0.4 | 0.4 |
| Internal friction angle | $\phi_{ef}$ [°] | - | 19 |
| Cohesion | $c_{ef}$ [kPa] | - | 23 |

### 4.1 Mohr-Coulomb model enhancement - small strain stiffness model.

The primary material model used in this study to reconstruct the current stress state is Mohr-Coulomb elastoplastic model. Its main drawback represents the assumption of the soil as linear elastic material until the shear failure occurs. The survey of the underground space showed no cracks or shear deformations, even in the areas where maximum stress deviator values were identified using the elastic predictive analysis. The lack of significant deformations or shear failures shows that the stress model should be chosen for that part of the material model that describes the material's stiffness. On the other hand, the need for advanced material parameters makes using the advanced material model difficult. Therefore, using the well-known Mohr-Coulomb model with the assumption of nonlinear isotropic elasticity for the small strain range would be convenient [10].

The model describes the stiffness using bulk and shear modulus and their development using the following equations:

$$G(E_d) = A + B\cos\left[\alpha\left(\log_{10}\left(\frac{E_d}{\sqrt{3}C}\right)\right)^{\gamma}\right], \tag{3}$$

$$K(\varepsilon_v) = A + B\cos\left[\delta\left(\log_{10}\left(\frac{|\varepsilon_v|}{T}\right)\right)^{\mu}\right], \tag{4}$$

$G(E_d)$ is the shear modulus, $K(\varepsilon_v)$ is the bulk modulus. $E_d$ and $\varepsilon_v$ are strain invariants, Fig. 3. The parameters $A$, $B$, $C$, $R$, $S$, $T$, $\alpha$, $\gamma$, $\delta$, $\mu$ are all material constants, Table 3. Still, the essential part is to determine the proper strain range that one can mark as a "small strain" region that bounds the evolution zone of these modules. A standard linear elastic model governs stress beyond this small strain range.

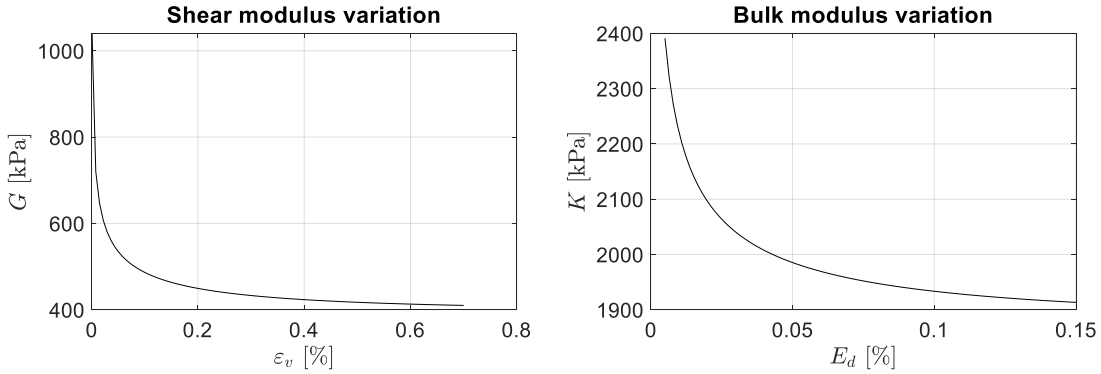


Fig. 3: Variation of shear and bulk modulus with accumulated values of strain invariants.

Table 3: Soil parameters for small strain model.

| Parameter | Value | Parameter | Value |
|---|---|---|---|
| $A$ | 420.0 | $R$ | 706.0 |
| $B$ | 390.0 | $S$ | 620.0 |
| $C$ | $5.0\times10^{-4}$ % | $T$ | $1.0\times10^{-3}$ % |
| $\alpha$ | 1.235 | $\delta$ | 2.169 |
| $\gamma$ | 0.595 | $\mu$ | 0.425 |
| $E_d$ - min | $9.0\times10^{-4}$ % | $\varepsilon_v$ - min | $1.0\times10^{-3}$ % |
| $E_d$ - max | 0.75 % | $\varepsilon_v$ - max | 0.14 % |
| $G$ | 410.00 kPa | $K$ | 1913.00 kPa |

### 4.2 The Current status of Čachtice underground

The current state of Čachtice underground corridors is displayed in the picture below, Fig. 4. The whole underground space is in loess soil. A few trees are on the surface, but these weren't considered in the calculation. During the visual inspection, the current state was found. Landslides, cracks, and deformations of the possible collapse of soil walls and vaults were wanted on the spot. But these problems weren't confirmed. Dangerous areas from the point of view of statics have been determined, on which numerical calculations were made in these places.

Fig. 4: The state of the Čachtice underground and a dangerous intervention in the statics.

### 4.3 Stability of the Čachtice underground in sections

In the first stage, the Linear Elastic constitutive model was used to recreate the potential stress state in the area of interest and to identify high-stress concentration in the given cross-section. One expects that the possible loss of stability occurs in the potential zones of high shear stress, Fig. 5, such as the heels of vaults, sharp angles, etc. These stresses, especially in the spaces above the vault, were entered into Table 4 as the most significant stresses at the points on the left and right sides. In our case, the vault is an essential part of the rock structure.

Table 4: Calculated stresses above the vault in numerical values in section 1.

| Sections | Vault | $\sigma_{xx}$ [kPa] | $\sigma_{yy}$ [kPa] | $\tau_{xy}$ [kPa] |
|---|---|---|---|---|
| 1 | On the left | 47.067 | 188.175 | 80.731 |
| | On the right | 21.188 | 74.359 | 42.645 |
| 2 | On the left | 100.025 | 125.370 | 82.362 |
| | On the right | 76.695 | 99.244 | 81.544 |
| 3 | On the left | 194.829 | 262.624 | 197.399 |
| | On the right | 264.651 | 187.826 | 166.060 |

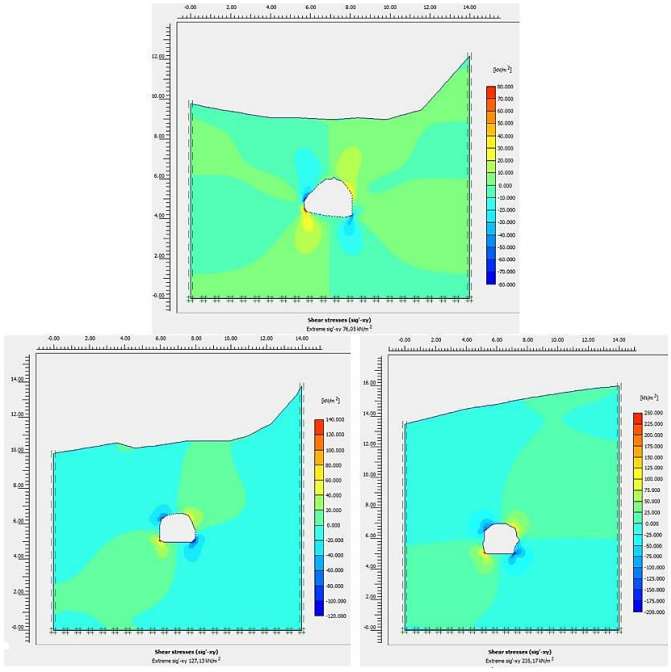

Fig. 5: Shear stresses in sections 1, 2, and 3.

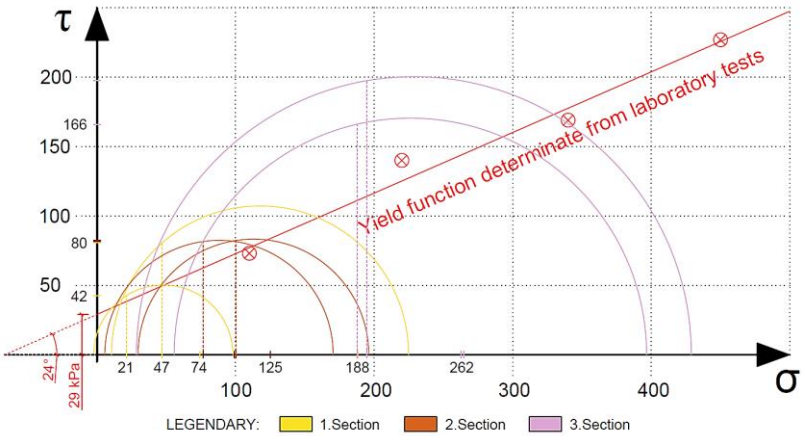


Fig. 6: Mohr circles in sections 1, 2, and 3.

Fig. 6 shows the plane of normal stress $\sigma$ on the horizontal axis and shear stress $\tau$ on the vertical axis. The yield boundary is described by shear parameters such as internal friction angle and cohesion. The values of shear parameters are shown in Table 1, and they can be determined according to STN 72 1030: Laboratory direct shear box drained test of soils, which was presented in detail by [8, 11-13]. Individual Mohr's circles are constructed from stresses calculated by PLAXIS, Table 4. The shear strength of the soil is lower than the shear stress. This means one should observe various deformations in the form of cracks/rapture in the given areas. However, the visual inspection did not observe such defects on the spot, caused by the soil consolidation and redistribution of the overshooting portion of stress into the nearby soil. A comparison of the stress field evaluated using the linear elastic model and the lack of ruptures or cracks showed that the yield parameters and actual stress field are lower than the one obtained by the linear elastic model. Such a comparison shows that overall stability should be satisfied using the elastoplastic model, which should accurately present the appropriate stress field.

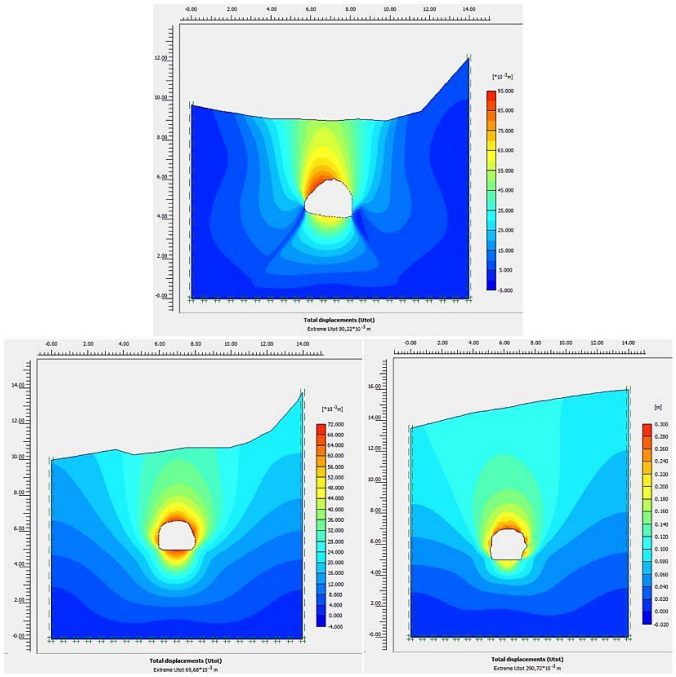

Fig. 7: Maximum deformations in sections 1, 2, and 3.

The Mohr-Coulomb constitutive model was adopted in the second stage of the calculation to calculate the appropriate stress field using former assumptions, Fig. 7. The maximum measured values in sections using Mohr-Coulomb constitutive model were 9, 7 and 29 cm. A calculation was performed to obtain the stress field only because one did not observe any movement or deformation, assuming the overall development over time, the soil body has already become balanced, and only

the stresses from this calculation were used in the next stage, zeroing the deformations. These assumptions are confirmed in the third step safety stage of the analysis, where the factor of safety *FS* = 1.642 was calculated for the first section. For the second section, the safety factor *FS* = 1.705 was calculated. The third section calculated the factor of safety *FS* = 1.383. The factor of safety values and direct observations showed that the complex underground system is stable without any sign of degradation or stability loss.

To preserve the stability of the portals and the natural appearance of the geostructure, it is possible to apply various raw materials presented in detail [14]. Repairs of the walls of the Čachtice underground by people from the civic association lead to the question of correctly designing the monitoring of such a geostructure [15]. Losing orientation in vast underground complexes is often harmful to health. One of the solutions to more effectively use the spaces not only of the Čachtice underground is its digital projection or spatial orientation [16]. We expect that digital projection is only one step in the digital age.

## 5 Conclusion

The Čachtice underground corridors are located in loess soil. A 3D model of these corridors was created, and three sections were determined in which numerical calculations were performed in Plaxis 2D software. The numerical analysis was separated into three phases, identifying shear stress concentration, identifying plastic zones, and calculating the factors of safety. The calculation of the Čachtice underground identified areas with increased shear stresses above the vaults using the linear elastic constitutive model. Crack/fissure-type defects should occur in these areas. Such defects were not visible on visual inspection.

Given that the Čachtice underground has been excavated for some century, we can assume that the calculated maximum deformations have already occurred over time. We claim the excavation is stable if the conditions do not change diametrically. This assumption is supported by the calculated factors of safety *FS* = 1.642; 1.705; 1.383, respectively. This article points out how we should proceed in other cases in the Čachtice underground.

## Acknowledgement

This research was funded by Operational Programme Integrated Infrastructure: Application of innovative technologies focused on the interaction of engineering constructions of transport infrastructure and the geological environment, ITMS2014+ code 313011BWS1. The project is co-funding by European Regional Development Fund.

## References

[1] MARSCHALKO, M. - DURAJ, M. - NIEMIEC, D. - YILMAZ, I. - PRYVALOV, A.: Churches influenced by underground mining in the Karvina region used for the purposes of geotourism. Procedia engineering, Vol. 161, 2016, pp. 2271-2275.
[2] Geological map of Slovakia, https://apl.geology.sk/gm50js/
[3] MARSCHALKO, M. - ZIĘBA, Z. - NIEMIEC, D. - NEUMAN, D. - MOŃKA, J. - DĄBROWSKA, J.: Suitability of Engineering-Geological Environment on the Basis of Its Permeability Coefficient: Four Case Studies of Fine-Grained Soils. Materials, Vol. 14(21), 2021, 6411.
[4] VALAŠKOVÁ, V. – VLČEK, J.: Determination of the deformation characteristics of the foam concrete as a sub-base. Journal of Vibroengineering: Theoretical & practical aspects of Vibration Engineering, Vol. 23, No. 1, 2021, pp. 156-166.
[5] DANANAJ, I. – KLUKANOVÁ, A. – LIŠČÁK, P.: Problems of monitoring of volume unstable soils and their properties: A case study Vesele. (in Slovak: Problematika monitoring objemovo nestálych zemín a ich vlastností – prípadová štúdia Veselé). Mineralia Slovaca, Vol. 44, 2012, pp. 461-472.
[6] CHROMČÁK, J. - GRINČ, M. - PÁNISOVÁ, J. - VAJDA, P. - KUBOVÁ, A.: Validation of sensitivity and reliability of GPR and microgravity detection of underground cavities in complex urban settings: Test case of a cellar. Contributions to Geophysics and Geodesy, Vol. 46, No. 1, 2016, pp. 13-32.
[7] MUSZYŃSKI, Z. - RYBAK, J.: Evaluation of terrestrial laser scanner accuracy in the control of hydrotechnical structures. Studia Geotechnica et Mechanica, Vol. 39(4), 2017.
[8] GAGO, F. - VLČEK, J. - VALAČKOVÁ, V. - FLORKOVÁ, Z.: Laboratory Testing of Kinetic Sand as a Reference Material for Physical Modelling of Cone Penetration Test with the Possibility of Artificial Neural Network Application. Materials, Vol. 15, No. 9, 2022, 3285.

[9] ONITSUKA, K. - HONG, Z. - HARA, Y. - YOSHITAKE, S.: Interpretation of oedometer test data for natural clays. Soils and foundations, Vol. 35, No. 3, 1995, pp. 61-70.
[10] STACHO, J. - SULOVSKA, M.: Numerical modelling of the subsoil zone between stone columns. Slovak Journal of Civil Engineering, Vol. 27(4), 2019, pp. 32-39.
[11] ABD AKRAM, H.: Preliminary Study on the Reduction in Shear Strength Parameters of Gypseous Soil upon Wetting. Civil and Environmental Engineering, Vol. 18, Iss. 1, 2022, pp. 195-199, doi: https://doi.org/10.2478/cee-2022-0018.
[12] STACHO, J. - SULOVSKA, M.: Shear Strength Properties of Coarse-Grained Soils Determined Using Large-Size Direct Shear Test. Civil and Environmental Engineering, Vol. 18, Iss. 1, 2022, pp. 244-257, doi: https://doi.org/10.2478/cee-2022-0023.
[13] STACHO, J. - SULOVSKA, M. - SLAVIK, I.: Determining the shear strength properties of a soil-geogrid interface using a large-scale direct shear test apparatus. Periodica Polytechnica Civil Engineering, Vol. 64(4), 2020, pp. 989-998.
[14] NGUYEN, G. - GRZYBOWSKA-PIETRAS, J. - BRODA, J.: Application of innovative ropes from textile waste as an anti-erosion measure. Materials, Vol. 14(5), 2021, 1179.
[15] SAVI, R. - CARRI, A. - CAVALCA, E. - VALLETTA, A.: Applicazione di un sistema di monitoraggio innovativo in una gallateria stradale danneggiata da un terremoto. IX IAGIG, Napoli 10-11 Maggio 2019.
[16] MIHÁLIK, M. - HRUBOŠ, M. - VESTENICKÝ, P. - HOLEČKO, P. - NEMEC, D. - MALOBICKÝ, B. MIHÁLIK, J.: A Method for Detecting Dynamic Objects Using 2D LiDAR Based on Scan Matching. Applied Sciences, Vol. 12, No. 11, 2022, 5641.